Cloud and Cloud Shadow Detection for Landsat Images: The Fundamental Basis for Analyzing Landsat Time Series

Chapter · May 2018

DOI: 10.1201/9781315166636-1

CITATIONS
14

READS
2,904

4 authors:

Zhe Zhu
University of Connecticut
55 PUBLICATIONS **7,779** CITATIONS
SEE PROFILE

Shi Qiu
University of Connecticut
21 PUBLICATIONS **317** CITATIONS
SEE PROFILE

Binbin He
University of Electronic Science and Technology of China
140 PUBLICATIONS **1,333** CITATIONS
SEE PROFILE

Chengbin Deng
Binghamton University
39 PUBLICATIONS **1,229** CITATIONS
SEE PROFILE

1

Cloud and Cloud Shadow Detection for Landsat Images: The Fundamental Basis for Analyzing Landsat Time Series

Zhe Zhu, Shi Qiu, Binbin He, and Chengbin Deng

CONTENTS

Brief Summary

Cloud and cloud shadow detection is the fundamental basis for analyzing Landsat time series. This chapter provides a comprehensive review of all the cloud and cloud shadow detection algorithms designed explicitly for Landsat images. This review provides guidance on the selection of cloud and cloud shadow detection algorithms for various applications using Landsat time series.

1.1 Introduction

Landsat satellites have been widely used for a variety of remote sensing applications, such as change detection (Collins and Woodcock, 1996; Xian et al., 2009), land cover classification (Homer et al., 2004; Yuan et al., 2005), biomass estimation (Zheng et al., 2004; Lu, 2005), and leaf area index retrieval (Chen and Cihlar, 1996; Fassnacht et al., 1997). Nevertheless, for decades, most of the analyses were based on a single or a few cloud free Landsat images acquired at different dates, due to the high cost of Landsat images prior to 2008 (Loveland and Dwyer, 2012). Free and open access to the entire Landsat archive in 2008 has changed the story entirely (Woodcock et al., 2008; Wulder et al., 2012). Landsat data are being downloaded for an unprecedented variety of applications. Many of them require frequent Landsat observations for the same location – Landsat Time Series (LTS). The Landsat Global Archive Consolidation (LGAC) initiative has added 3.2 million Landsat images to the U.S. Geological Survey (USGS) Earth Resources Observation and Science (EROS) Center (Wulder et al., 2016), which has made time series analysis with LTS even more popular. Decreasing data storage costs and increasing computing power have further stimulated the use of LTS.

Though time series analysis based on LTS has attracted much attention, automated cloud and cloud shadow detection has been and remains a major obstacle. The presence of clouds and cloud shadows reduces the usability of the Landsat image which makes it difficult for any kind of remote sensing applications. For coarse resolution images, such as from the Advanced Very High Resolution Radiometer (AVHRR) and Moderate Resolution Imaging Spectroradiometer (MODIS), there are many mature operational algorithms for detecting clouds and cloud shadows (Derrien et al., 1993; Ackerman et al., 1998). However, for moderate resolution satellites, like Landsat, there were no algorithms that could provide cloud and cloud shadow masks at the pixel level. This is not surprising because Landsat images were not affordable, each of which previously cost more than 400 U.S. dollars per image. Even when cloudy Landsat images are used, most of the time only

a small number of images are needed, and manual interpretation of clouds and their shadows in the images is feasible. However, when these financial constraints were lifted (Woodcock et al., 2008), an unprecedented demand arose for automatically processing a massive number of Landsat images for time series analysis. Manual interpretation of cloud and cloud shadow was no longer acceptable.

1.2 Landsat Data and Reference Masks

1.2.1 Landsat Data

Since 1972, Landsat satellites have provided a continuous Earth observation data record. Landsats 1–5 carried the Multispectral Scanner System (MSS) sensor with 60-meter spatial resolution. The MSS only collected images with four spectral bands, including green, red, and two Near InfraRed (NIR) bands (Table 1.1). Note that the Landsat 3 MSS also included a Thermal Infrared (TIR) band, but failed shortly after launch. The fewer bands result in known difficulties in detecting clouds and cloud shadows (Braaten et al., 2015). However, the MSS images are still crucial for LTS related analyses (Pflugmacher et al., 2012). Since the launch of Landsat 4 in 1982, the Thematic Mapper (TM) has provided more spectral information at 30-meter spatial resolution (Table 1.1). The TM sensor was also carried on Landsat 5, which was launched on March 1, 1984, and functioned for over 28 years until 2012. Landsat 7, carrying the Enhanced Thematic Mapper Plus (ETM+), was launched on April 15, 1999 (Table 1.1). This instrument also has a 30-meter spatial resolution and improved radiometric and geometric calibration accuracies, but the Scan Line Corrector (SLC) has failed since May 31, 2003. Both TM and ETM+ have a TIR band at a spatial resolution of 120-meter and 60-meter, respectively. Landsat 8 was launched on February 11, 2013. It has two sensors: Operational Land Imager (OLI) and Thermal Infrared Sensor (TIRS) (Table 1.1). The OLI instrument provides 30-meter resolution optical data, while TIRS provides 100-meter resolution TIR data. Note that the TIRS has a shorter design life compared to the OLI. Additionally, the new OLI added the new blue band (Band 1: 0.435–0.451 μm) and the cirrus band (Band 9: 1.363–1.384 μm) with 30-meter spatial resolution.

Although each Landsat satellite can cover global land every 16 days, many of the observations are inevitably impacted by clouds and cloud shadows. Figure 1.1 illustrates mean global cloud cover calculated based on all available Landsat 8 daytime images acquired between September 2013 and August 2017. The cloud cover information for each Landsat Path/Row is calculated based on the metadata of Landsat 8 images downloaded from the USGS Landsat Bulk Metadata Service (https://landsat.usgs.gov/landsat-bulk-metadata-service), which is derived based on an algorithm called Fmask

TABLE 1.1

Landsat 1–5 MSS, Landsat 4–5 TM, Landsat 7 ETM+ and Landsat 8 OLI Sensor Characteristics

Landsat 1–5 MSS Bands (μm)	Landsat 4–5 TM Bands (μm)	Landsat 7 ETM+ Bands (μm)	Landsat 8 OLI/TIRS Bands (μm)
	Band 1 (0.45–0.52)	Band 1 (0.45–0.52)	Band 1 (0.435–0.451)
Band 4 (0.50–0.60)	Band 2 (0.52–0.60)	Band 2 (0.52–0.60)	Band 2 (0.452–0.512)
Band 5 (0.60–0.70)	Band 3 (0.63–0.69)	Band 3 (0.63–0.69)	Band 3 (0.533–0.590)
Band 6 (0.70–0.80)	Band 4 (0.76–0.90)	Band 4 (0.77–0.90)	Band 4 (0.636–0.673)
Band 7 (0.80–1.10)			
	Band 5 (1.55–1.75)	Band 5 (1.55–1.75)	Band 5 (0.851–0.879)
Band 8 (10.40–12.50) Landsat 3 only[a]	Band 6 (10.40–12.50)	Band 6 (10.40–12.50)	Band 6 (1.566–1.651)
	Band 7 (2.08–2.35)	Band 7 (2.09–2.35)	Band 7 (2.107–2.294)
		Band 8 (0.52–0.90)	Band 8 (0.503–0.676)
			Band 9 (1.363–1.384)
			Band 10 (10.60–11.19)
			Band 11 (11.50–12.51)

[a] Indicates that the thermal band of the Landsat 3 MSS was unsuccessful and not available.

(Zhu and Woodcock, 2012; Zhu et al., 2015). Extremely high cloud cover is observed in tropical rainforest regions, while for arid places, such as desert or dryland regions, cloud cover is relatively low. The mean global cloud cover contained in the Landsat images is approximately 41.59%, which means that clouds impact almost half of the Landsat observations.

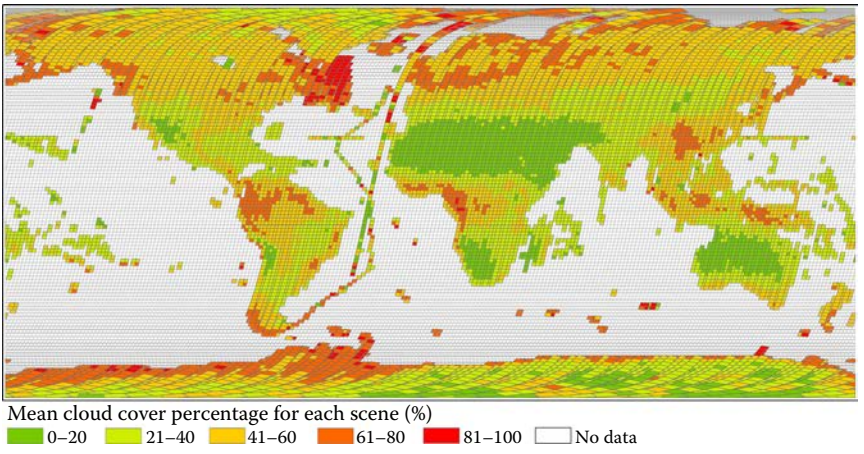

FIGURE 1.1
Mean global cloud cover percentage calculated based on all available Landsat 8 images acquired between September 2013 and August 2017. A total of 966,708 Landsat 8 images are used. The mean global cloud cover percentage from all Landsat 8 observations is 41.59%.

1.2.2 Manual Masks of Landsat Cloud and Cloud Shadow

Manually interpreted cloud and cloud shadow masks are the most important data source for developing and/or validating the cloud and cloud shadow detection algorithms (Irish et al., 2006; Zhu and Woodcock, 2012; Hughes and Hayes, 2014; Foga et al., 2017; Qiu et al., 2017). At present, there are three publicly available, manually interpreted cloud and cloud shadow masks derived from Landsat images (Table 1.2), including "L7 Irish" masks for Landsat 7 data (USGS, 2016a), "L8 SPARCS" masks for Landsat 8 data (USGS, 2016b), and "L8 Biome" masks for Landsat 8 data (USGS, 2016c). These masks are manually interpreted based on Landsat images randomly selected from different locations, which cover a variety of land cover types, and the cloud cover percentage within each manual mask also varies substantially. The "L7 Irish" manual masks were first created to systematically cover the global environments and different cloud conditions (Irish et al., 2006). The "L7 Irish" masks were produced based on Landsat 7 ETM+ images by visual interpretation of full resolution images with different Landsat band combinations, and their average error was estimated at approximately 7% (Oreopoulos et al., 2011). The "L8 SPARCS" manual masks were created manually from Landsat 8 OLI images by Hughes and Hayes (2014), which was used to validate Spatial Procedures for Automated Removal of Cloud and Shadow (SPARCS) algorithm. Note that those manual cloud and cloud shadow masks are provided at a 3 km by 3 km Landsat subset (1000 × 1000 30-meter pixels), with around 4% of pixels being ambiguous (Foga et al., 2017). The manual cloud and cloud shadow masks in "L8 Biome" are designed for Landsat 8 OLI/TIRS images, which were randomly selected from different locations around the world using a biome-based stratified sampling approach. Their corresponding cloud and cloud shadow masks were produced by multiple visual criteria (such as brightness, shape, and texture) with various band combinations by a single analyst (Foga et al., 2017). This new dataset achieved better accuracy than the "L7 Irish," due to the multiple visual criteria it used (Foga et al., 2017).

TABLE 1.2

Manual Cloud and Cloud Shadow Masks Derived from Landsat Images

Name	Sensor	Number of Images	Date Range		Error	Reference
			Start	End		
L7 Irish	ETM+ (SLC on)	206 (45)	06/06/2000	12/30/2001	7.00%	USGS (2016a)
L8 SPARCS	OLI	80 (80)	05/12/2013	11/02/2014	4.00%	USGS (2016b)
L8 Biome	OLI	96 (33)	04/13/2013	11/05/2014	Less than 7.00%	USGS (2016c)

Note that the all images contain manual cloud masks. The numbers in the brackets indicate the number of cloud shadow masks for each dataset.

1.3 Cloud and Cloud Shadow Detection Based on a Single-Date Landsat Image

Recently, many cloud and cloud shadow detection algorithms have been developed for Landsat images (Table 1.3). Among them, some were proposed by using a single-date Landsat image (hereafter single-date algorithms), and we can classify these single-date algorithms into two categories: physical-rules-based and machine-learning-based algorithms (Table 1.3).

1.3.1 Physical-Rules-Based Cloud and Cloud Shadow Detection

1.3.1.1 Physical-Rules-Based Cloud Detection Algorithms

The physical-rules-based algorithms detect clouds by identifying their physical characteristics of clouds, that are "bright", "white", "cold", and "high" (Irish, 2000; Zhu et al., 2015). Compared to other land cover types, the reflectance of cloud is much higher in almost all wavelengths, which makes clouds look "bright". Therefore, we can use some simple thresholds in the spectral bands to exclude clear sky pixels that are not bright enough. Clouds are "white" due to the similar reflectance in all wavelengths, particularly in the visible bands. In this case, some indices such as "whiteness" (Zhu and Woodcock, 2012), Normalized Difference Vegetation Index (NDVI), and Normalized Difference Snow Index (NDSI) can be used to separate clouds from clear sky pixels that are not white enough. Moreover, clouds are "cold" because they are usually high in the air, and the temperature of clouds follows the environmental lapse rate—the higher the clouds, the colder the temperature. This characteristic can be successfully captured by the thermal band from Landsat TM, ETM+, and TIRS instruments, which can further separate clouds from similar bright and white land surfaces (e.g., barren sand, soil, rock, snow/ice, etc.). Additionally, as clouds are usually "high" in the sky, the path for water vapor over clouds is much shorter than that for places without clouds. Therefore, the water vapor absorption band (or the cirrus band) is especially helpful in identifying higher altitude clouds.

Most of the algorithms are developed for Landsat TM and ETM+ images. Historically, the Automated Cloud Cover Assessment (ACCA) was used to provide cloud cover percentage in Landsat TM and ETM+ images (Irish, 2000; Irish et al., 2006). With several spectral filters, ACCA works well for estimating a cloud cover score for each image but is not sufficiently precise in identifying the locations and boundaries of clouds (Zhu and Woodcock, 2012). Besides, ACCA fails to identify warm cirrus clouds and may misidentify snow/ice as clouds, mainly because the static thresholds in ACCA are insufficient to capture the various kinds of clouds and the variety of land surface types. To better distinguish cloud from snow/ice, Choi and Bindschadler (2004) used the cloud and cloud shadow geometry matching approach iteratively

TABLE 1.3

Characteristics of Different Cloud and Cloud Shadow Detection Algorithms for Landsat Images

Category	Algorithm Name	Landsat Sensor	Cloud/ Shadow	Ancillary Data	Overall Accuracy	Reference
Single-date: Physical rules	MFmask	TM ETM+ OLI/TIRS	Both	DEM	96%	Qiu et al. (2017)
	LSR 8	OLI/TIRS	Both	N/A	N/A	Vermote et al. (2016)
	UDTCDA	OLI/TIRS	Cloud	MOD09A1	N/A	Sun et al. (2016)
	MSScvm	MSS	Both	DEM	84%	Braaten et al. (2015)
	ELTK	OLI/TIRS	Cloud	N/A	N/A	Wilson and Oreopoulos (2013)
	Fmask	TM ETM+ OLI/TIRS	Both	N/A	96%	Zhu and Woodcock (2012), Zhu et al. (2015)
	N/A	TM ETM+	Both	DEM	88%∼99%	Huang et al. (2010)
	LTK	TM ETM+ OLI/TIRS	Cloud	N/A	93%	Oreopoulos et al. (2011)
	LEDAPS	TM ETM+	Both	Air temperature from NCEP	N/A	Vermote and Saleous (2007)
	CDSM/ANTD	ETM+	Both	N/A	N/A	Choi and Bindschadler (2004)
	ACCA	TM ETM+ OLI/TIRS	Cloud	N/A	N/A	Irish (2000), Irish et al. (2006)
Single-date: Machine learning	N/A	OLI	Cloud	N/A	N/A	Zhou et al. (2016)
	SPARCS	ETM+	Both	N/A	99%	Hughes and Hayes (2014)
	See5	OLI	Cloud	N/A	89%	Scaramuzza et al. (2012)
	AT-ACCA	OLI	Cloud	N/A	90%	Scaramuzza et al. (2012)
	N/A	ETM+	Both	N/A	N/A	Potapov et al. (2011)
	N/A	ETM+	Cloud	N/A	N/A	Roy et al. (2010)
	N/A	MSS	Cloud	N/A	93%	Lee et al. (1990)

(*Continued*)

TABLE 1.3 (*Continued*)

Characteristics of Different Cloud and Cloud Shadow Detection Algorithms for Landsat Images

Category	Algorithm Name	Landsat Sensor	Cloud/ Shadow	Ancillary Data	Overall Accuracy	Reference
Multi-date	IHOT	MSS TM ETM+	Cloud	N/A	N/A	Chen et al. (2015)
	Tmask[a]	TM ETM+ OLI/TIRS	Both	N/A	N/A	Zhu and Woodcock (2014)
	N/A[a]	TM ETM+	Both	N/A	97%	Goodwin et al. (2013)
	N/A	TM ETM+	Both	N/A	N/A	Jin et al. (2013)
	MTCD[a]	TM ETM+	Both	Sentinel-2 data	N/A	Hagolle et al. (2010)
	N/A	TM	Both	N/A	N/A	Wang et al. (1999)

Note: MFmask: Mountainous Fmask; LSR 8: Landsat 8 Surface Reflectance product; UDTCDA: Universal Dynamic Threshold Cloud Detection Algorithm; MSScvm: MSS clear-view-mask; ELTK: Enhanced LTK; Fmask: Function of mask; LTK: Luo Trishchenko Khlopenkov; LEDAPS: Landsat Ecosystem Disturbance Adaptive Processing System; CDSM/ANTD: Cloud Detection using Shadow Matching/Automatic NDSI Threshold Decision; ACCA: Automatic Cloud Cover Assessment; SPARCS: Spatial Procedures for Automated Removal of Cloud and Shadow; See5: C5.0 algorithm used to generate a decision tree. AT-ACCA: Artificial Thermal-Automated Cloud Cover Algorithm; IHOT: Iterative Haze Optimized Transformation; Tmask: multiTemporal mask; MTCD: Multi-Temporal Cloud Detection; TM: Thematic Mapper; ETM+: Enhanced Thematic Mapper Plus; OLI: Operational Land Imager; TIRS: Thermal Infrared Sensor; DEM: Digital Elevation Model; MOD09A1: MODerate resolution Imaging Spectroradiometer surface reflectance product; NCEP: National Centers for Environmental Prediction.

[a] Indicates the algorithms based on Landsat time series.

to determine the optimal threshold of NDSI for each Landsat image in cloud detection. This approach works well over ice sheets, but it is time-consuming and only works on the surface of ice sheets. Vermote and Saleous (2007) proposed a cloud detection algorithm for Landsat TM and ETM+ images, and the detection results are provided as one of the internal products in the Landsat Ecosystem Disturbance Adaptive Processing System (LEDAPS) atmosphere correction software. This algorithm needs surface temperature from the National Centers for Environmental Prediction (NCEP) as ancillary data to generate a surface temperature reference layer for cloud detection. Huang et al. (2010) constructed a spectral temperature space to identify clouds in Landsat image using clear sky forest pixels as a reference. This method works well over forest areas but has not been fully tested for non-forest areas. By revisiting the Luo Trishchenko Khlopenkov (LTK) scene identification algorithm initially developed for the MODIS image (Luo et al., 2008), Oreopoulos et al. (2011) modified this algorithm to detect clouds in Landsat 7 ETM+ data using simple thresholds derived for the blue, red, NIR, and Short-Wave Infrared (SWIR) bands (no thermal band). Recently, Zhu and Woodcock (2012) developed the Fmask (Function of mask) algorithm that detects cloud by using a scene-based threshold. This method is suitable for the Landsats 4–8 data and can generate a cloud probability layer. Users can adjust the threshold of cloud probability to determine cloud masks. The default threshold (global optimal) is 22.5%. If large omissions are found, a smaller threshold (e.g., 12.5%) is recommended, and if large commissions are observed, a higher threshold (e.g., 50%) is recommended. This method has also been successfully integrated into the Landsat surface reflectance Climate Data Record (CDR) and Collection 1 Quality Assessment (QA) band provided by the USGS Earth Resources Observation and Science (EROS) Center. In the Fmask algorithm, the thermal band is one of the important inputs, as it can capture the "cold" character of clouds (Zhu et al., 2015). However, the temperature for clear sky pixels can also vary widely due to substantial changes in elevation, and this will lead to commission and omission errors in cloud detection in mountainous areas. To reduce this issue, Qiu et al. (2017) provided a Mountainous Fmask (MFmask) algorithm that normalizes the thermal band with Digital Elevation Models (DEMs) based on a simple linear temperature-elevation model.

There are also algorithms explicitly designed for Landsat 8 images, many of which take advantage of the new blue and cirrus bands equipped in Landsat OLI. Wilson and Oreopoulos (2013) further modified the aforementioned LTK algorithm by including the cirrus band to detect cloud better. Zhu et al. (2015) also designed a cloud detection algorithm for Landsat 8 images by calculating a thin cloud probability layer from the cirrus band, and achieved better accuracy than the Fmask algorithm designed initially for TM and ETM+ images. Vermote et al. (2016) proposed a new cloud detection algorithm for Landsat 8, which used the inversion "residual" from the two blue bands and the cirrus band reflectance. To minimize the influences of cloud detection

from mixed pixels, complex surface structures, and atmospheric factors, Sun et al. (2016) presented a Universal Dynamic Threshold Cloud Detection Algorithm (UDTCDA) for Landsat 8 OLI images, but only the blue, green, red, NIR, and SWIR bands were used. The dynamic threshold in this method was determined based on MODIS monthly surface reflectance database, which was established based on the long-time series of MODIS 8-day synthetic surface reflectance products.

Very few algorithms have been designed for the Landsat MSS image, due to the limited number of spectral bands within the MSS sensor. To address this issue, Braaten et al. (2015) proposed a simple and automated cloud detection algorithm relying on green band brightness and the normalized difference between the green and red bands and achieved comparable accuracies to the Fmask algorithm.

1.3.1.2 Physical-Rules-Based Cloud Shadow Detection Algorithms

Detecting cloud shadows for Landsat images is more difficult than detecting clouds due to the spectral similarity of cloud shadows and dark surfaces. Cloud shadows are usually detected based on physical rules derived from the cloud shadow geometry.

Previously, the cloud shadow detection algorithms were developed based on simple spectral tests according to the dark features. However, it is difficult to directly use thresholds to determine cloud shadows because their spectral signatures are very similar to other dark surfaces (e.g., terrain shadows, wetlands, dark urban, etc.). Fortunately, the geometry-based cloud shadow detection has shown relatively good results. The geometry-based cloud shadow detection approach is based on the projection of cloud object onto the local plane of the Earth with respect to a direction of incoming solar radiation (Berendes et al., 1992; Le Hégarat-Mascle and André, 2009; Simpson et al., 2000). The relative positions of the sun, the satellite, and the cloud can be used to predict the cloud shadow observed in the satellite images (Figure 1.2). Methods for detecting cloud shadow based on geometry can be grouped into two categories: shape-similarity-match and cloud-height-estimation.

The shape-similarity-match approach detects cloud shadow by matching cloud shadows with cloud objects, assuming that cloud and cloud shadow shape are similar (Gurney, 1982; Berendes et al., 1992). Gurney (1982) assumed that a cumulus cloud is approximated in shape by its associated shadow and matched cloud shadows with clouds. Berendes et al. (1992) developed a semi-automated methodology for estimating cumulus cloud base height using Landsat data by matching cloud edges with their corresponding shadow edges. Due to the absence of the thermal band, Braaten et al. (2015) used cloud projection to identify cloud shadow in Landsat MSS image based on their geometry information. Although the computation of cloud and cloud shadow match is time-consuming and may result in some mismatches, this approach

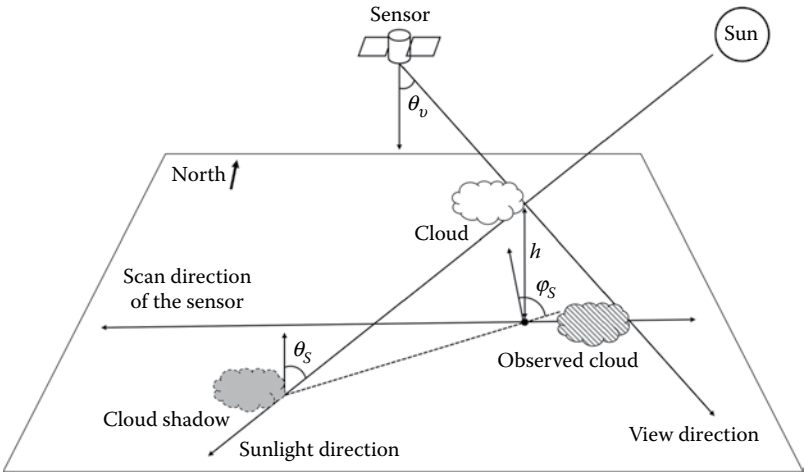

FIGURE 1.2
Sun/cloud/shadow geometry in Landsat image. Note that θ_s is the solar zenith angle, φ_s is the solar azimuth angle, θ_v is the satellite view zenith angle, and h is the cloud height. The position of the real cloud may shift from the cloud directly observed by the Landsat sensor.

is still an attractive routine, especially for images without the thermal band (e.g., Landsat MSS).

The cloud-height-estimation method uses a constant lapse rate to estimate cloud top height based on the Brightness Temperature (BT) difference between cloud top and the land surface. When the cloud height is known, the clouds can be easily projected to predict their associate shadows on the ground based on their geometry relationship (Vermote and Saleous, 2007; Huang et al., 2010). Vermote and Saleous (2007) detected cloud shadow for Landsat data using a geometric determination of shadow based on the cloud mask and the estimated altitude of cloud derived from the BT and a conversion factor range. Huang et al. (2010) identified cloud shadow based on the dark spectral features, the temperature-based cloud height estimation with a constant lapse rate, and the solar illumination geometry. Those methods can work well for thick clouds but are less ideal for the semitransparent clouds, of which the BT will be a mixture of thin cloud and the surface underneath.

Zhu and Woodcock (2012) and Zhu et al. (2015) calculated cloud shadows by combining the previous shape-similarity-matching and the cloud-height-estimation methods, and treated the cloud as a 3D object. This algorithm works well for most cases, but it may fail to detect the correct cloud shadows for places of large topographic change and terrain shadows. To address those issues, Qiu et al. (2017) applied a double-projection method to calculate cloud shadow shape and removed terrain shadows using a topographic correction model with the aid of DEMs. In addition, this improved Fmask algorithm can estimate a more accurate cloud height based on heights estimated from neighboring clouds, that also improves the detection of cloud shadow for Landsat images.

1.3.2 Machine-Learning-Based Cloud and Cloud Shadow Detection

Regarding the machine-learning-based algorithms, clouds and/or cloud shadows are generally treated as a cover type and are identified using a certain classifier trained by previously collected training dataset – supervised classification. Lee et al. (1990) combined texture-based features in a network to discriminate clouds in Landsat MSS images and achieved an overall cloud identification accuracy of 93%. Recognizing that omission and commission errors for cloud detection will always occur in large datasets for ACCA, Roy et al. (2010) implemented both the ACCA algorithm and a classification tree approach to detect clouds using a large number of training pixels from a global Landsat Level 1G database. Potapov et al. (2011) also manually selected lots of cloud pixels as training data based on 21 Landsat images from different years and different regions and built a single tree model for cloud type to classify the clouds. Due to the possible loss of the thermal band on Landsat 8, Scaramuzza et al. (2012) expanded the ACCA pass-1 algorithm without the use of the thermal band, identifying clouds for Landsat 8 through a statistical classifier C5.0 (a classification tree) based on many randomly sampled pixels from a series of training images. Hughes and Hayes (2014) also explored the inclusion of spatial information as an input to a neural network classifier on identifying and classifying clouds for Landsat images. Zhou et al. (2016) utilized the traditional threshold to obtain a coarse cloud mask and then used the Support Vector Machine (SVM) classifier to detect clouds in Landsat 8 images. Though all these investigations pointed out the usefulness of machine-learning-based methods in cloud detection, most require a certain level of knowledge of cloud or surface conditions within the images (as training data) and commonly fail to detect clouds for certain unique conditions (Huang et al. 2010). Additionally, cloud shadow in Landsat image can also be detected using the machine-learning-based methods (Potapov et al., 2011; Hughes and Hayes, 2014). This method, however, heavily relies on the training dataset and has substantial omission or commission errors (Hughes and Hayes, 2014).

1.4 Cloud and Cloud Shadow Detection Based on Multitemporal Landsat Images

In addition to the single-date algorithm, cloud and cloud shadow detection algorithms based on multitemporal Landsat images have also been developed (hereafter multitemporal algorithm). Compared to the spectral or spatial features derived from a single-date Landsat image, multitemporal Landsat images can provide extra-temporal information in cloud and cloud shadow detection, and are reported to produce better cloud and cloud shadow masks

(Table 1.3). The basic idea of these algorithms is that clouds and cloud shadows can be easily detected by comparing an observed image with a clear sky reference (image differencing), as the presence of clouds and cloud shadows will result in sudden changes of Landsat reflectance (Wang et al., 1999; Jin et al., 2013).

1.4.1 Cloud Detection Based on Multitemporal Landsat Images

For a long time, multitemporal cloud detection algorithms were only based on two-date or multi-date Landsat images. Early on, Wang et al. (1999) proposed the use of two-date Landsat TM images to find clouds by image differencing. This proposed method first coarsely finds the clouds for the two Landsat TM images by setting a histogram-derived threshold for the brightness values, and then uses another static threshold for the absolute brightness difference between the two images to further ensure reliable cloud detection. Jin et al. (2013) identified clouds by incorporating Landsat blue and thermal bands from two-date images. Based on two Landsat images that have no overlapping clouds, this method first selected the relaxed clouds by differencing the blue bands from the two images and then produced the restricted clouds by eliminating some commission pixels with relatively low spectral values in the SWIR band and low temperature in the thermal band. The thresholds used in this approach were determined by measuring spectral deviation from the mean value of the input images. These methods can accurately detect cloud for the reported images, but the thresholds may not be transferable to other images. To avoid confusion between bright surfaces and haze/cloud, Chen et al. (2015) proposed an Iterative Haze Optimized Transformation (IHOT) for improving haze/clouds detection for Landsat images with the help of a corresponding clear image. By integrating an iterative procedure of regressions into the HOT (Zhang et al., 2002), the reflectance difference between hazy and clear images, and reflectance of hazy and clear images, the land surface information can be removed. The IHOT result is derived to characterize the haze contamination on Landsat images spatially. These proposed approaches are practical and straightforward only using two-date or multi-date Landsat images but heavily dependent on the quality and availability of reference images. Besides, these approaches may not work well if extensive land cover changes occurred between the acquisition dates of the reference and cloudy images.

With free and open access to the Landsat archive, time series analysis with Landsat images became possible, providing a new way to detect clouds based on higher frequency Landsat observations. The LTS itself can be used for detecting clouds. Goodwin et al. (2013) used LTS from TM/ETM+ to detect clouds. By using the minimum and median values of the blue band as a reference, this algorithm can produce better cloud masks across Queensland compared to Fmask (Zhu and Woodcock, 2012). However, it has not yet been tested in environments with different soils, vegetation

cover, and structure or areas with snow/ice cover (Goodwin et al., 2013). Specifically designed for monitoring land cover change, an algorithm called Tmask (multitemporal mask) has been developed for automated masking of cloud and snow for LTS (Zhu and Woodcock, 2014). This method estimated time series models for each pixel based on "clear-sky LTS" previously filtered by the Fmask algorithm. By using a robust fitting approach, the cloud observations that are missed by Fmask will have minimal impacts on the estimation of the time series models. By comparing the model estimates with actual Landsat observations for the green, NIR, and SWIR bands, we will be able to detect any remaining cloud observations for the entire stack of Landsat images. In addition to the Landsat images, there are also algorithms developed for Landsat-like data, such as VENμS and Sentinel-2. Hagolle et al. (2010) developed the Multi-Temporal Cloud Detection (MTCD) method that detects sudden increases of reflectance in the blue band on a pixel-by-pixel basis using time series observations and tested the linear correlation of pixel neighborhoods taken from pairs of images acquired successively. The MTCD method provides better discrimination of cloudy and clear sky pixels than the ACCA method for Landsat images. However, it requires satellite data with high revisit frequency and sequential processing of the data.

1.4.2 Cloud Shadow Detection Based on Multitemporal Landsat Images

Most cloud shadow detection algorithms using multitemporal Landsat images assume that the presence of cloud shadows will lead to darker, colder, and smoother features than the regular land surface (Irish, 2000; Le Hégarat-Mascle and André, 2009). Wang et al. (1999) presented a wavelet transform approach to detect cloud shadows for two Landsat TM images automatically. Considering that the brightness changes of the cloud shadow-obscured regions are much smoother than the regions with no shadows, the absolute wavelet coefficients corresponding to cloud shadows decrease much greater amount than those of other regions. Thus, a relative contrast difference for the added result of the wavelet transform outputs was directly used to detect cloud shadow for the two Landsat images with a static threshold. Different from this complicated approach, Jin et al. (2013) detected the cloud shadows simply by differencing the SWIR and the thermal bands from two-date Landsat images and employed the geometric relationship between clouds and their corresponding shadows to reduce false positive errors. Zhu and Woodcock (2014) also identified cloud shadows for LTS by image differencing. The reference values were predicted using a time series model for each pixel. Though there are only a few cloud shadow detection approaches using multitemporal Landsat images, these methods can provide better results than the approaches based on a single-date Landsat image, especially for shadows from thin clouds (Zhu and Woodcock, 2014).

1.5 Discussions

1.5.1 Comparison of Different Algorithms

With so many different cloud and cloud shadow detection algorithms available in the literature, it is essential to compare those approaches and to provide further guidance on the selection of algorithms for those interested in using LTS. A list of most of the automated cloud and cloud shadow detection algorithms can be found in Table 1.3. We observe that the most widely used detection algorithms are based on a single-date Landsat image, probably due to the ease of implementation. Recently, Foga et al. (2017) compared the performances of several popular algorithms using 278 unique cloud validation masks over the entire globe and found that the CFmask (Fmask algorithm programmed in C) has the best overall accuracy for Landsat data. It should be noted that the methods based on multitemporal Landsat images can provide more accurate detection of cloud and cloud shadow, which is especially important for time series analysis (e.g., forest disturbance, land cover change, etc.) (Goodwin et al., 2013; Zhu and Woodcock, 2014).

1.5.2 Challenges

Clouds are easily confused with snow/ice, especially for mountaintop snow/ice (Selkowitz and Forster, 2015). These kinds of commissions can be reduced by the NDSI threshold (Zhu and Woodcock, 2012), verification of clouds with their corresponding shadows (Choi and Bindschadler, 2004), temperature normalization (Qiu et al., 2017), or composition of temporal pixels in summer season (Selkowitz and Forster, 2015). However, it is still difficult to separate clouds from snow in some circumstances (e.g., icy clouds).

The cloud shadow detection accuracy is still relatively low. The geometry projection of cloud is a good way to detect cloud shadow, but relies heavily on the previously identified cloud masks, which have commission or omission errors and subsequently result in inaccurate cloud shadows. In addition, the cloud shadows are commonly confused with other dark features, such as wetlands, dark urban, and terrain shadows. Terrain shadows can be removed using the topographic correction model with the aid of DEMs (Jin et al., 2013; Braaten et al., 2015; Qiu et al., 2017). The misidentification of cloud shadow contributed from other dark features can also be corrected based on the contextual information from the clouds' heights estimated from neighboring clouds (Qiu et al., 2017).

The use of multitemporal Landsat images can produce better cloud and cloud shadow masks by differencing new observations with reference observations. However, this kind of approach may not work well due to the range of non-cloud related variations in reflectance, such as the illumination

geometry, land surface change, geometric misregistration, and variation in radiometry or atmospheric composition (Hagolle et al., 2010; Goodwin et al., 2013; Zhu and Woodcock, 2014). Furthermore, these algorithms are computationally expensive compared to cloud and cloud shadow detection algorithms based on a single-date Landsat image.

1.5.3 Future Development

1.5.3.1 Spatial Information

When designing cloud and cloud shadow detection algorithms for Landsat images, the spectral information and the temporal information have been explored extensively, but the information contained in the spatial domain is less studied (Gurney, 1982; Martins et al., 2002). We expect that more cloud and cloud shadow detection algorithms will focus on the spatial characteristics of clouds and their shadows and provide masks at higher accuracies.

1.5.3.2 Temporal Frequency

The approaches based on multitemporal Landsat images can provide more accurate cloud and cloud shadow masks, when compared to the single-date approaches (Goodwin et al., 2013; Zhu and Woodcock, 2014). In addition to Landsat data, other Landsat-like satellites have also been launched, such as Sentinel-2A/2B. The integration of multi-source images will allow more frequent observations and further improve the detection accuracy. One major restriction of the multitemporal cloud and cloud shadow detection algorithms is that these algorithms require large amounts of data and computation time. However, this will be less an issue with the rapid development of computation technology.

1.5.3.3 Haze/Thin Cloud Removal

Compared with thick clouds, thin clouds are transparent, and images covered by thin clouds include information from both the atmospheric and the ground underneath (Li et al., 2012). This gives us the opportunity to remove the impacts of haze/thin clouds. If the satellite sensor profile and the atmospheric properties are known, haze/thin clouds' impacts can be reduced by atmospheric correction (Vermote and Saleous, 2007). However, it is difficult to acquire all the atmospheric properties (Liang et al., 2001), and atmospheric correction may fail in handling the locally concentrated thin clouds (Shen et al., 2014). Methods based on multispectral transformation, such as Tasseled Cap (TC) transformation (Richter, 1996), HOT (Zhang et al., 2002), and Advanced HOT (AHOT) (Liu et al., 2011), can remove haze/thin clouds' impacts effectively. Besides, haze/thin clouds are generally distributed in the low frequency parts of the image, which can be removed by using a low-pass filter (Shen et al., 2014), such as Wavelet Analysis (WA)

(Du et al., 2002) and Homomorphic Filter (HF) (Fan and Zhang, 2011). While many haze/thin cloud removal methods are available, there are still difficulties in automated identification of haze/thin clouds using current cloud detection algorithms. This will hamper the broad applications of haze/thin cloud removal approaches.

1.6 Conclusion

Clouds and cloud shadows are a pervasive, dynamic, and unavoidable issue in Landsat images, and their accurate detection is the fundamental basis for analyzing LTS. Many cloud and/or cloud shadow detection algorithms have been proposed in the literature. For cloud detection, most approaches are based on a single-date Landsat image, which rely on physical-rules or machine-learning techniques. With the policy of free and open Landsat data, some automated cloud detection methods were developed based on multitemporal Landsat images and can achieve better results. For cloud shadow detection, the geometry-based approach is widely used in the single-date algorithms. Meanwhile, by using multitemporal Landsat images, some researchers used the image differencing method to better identify cloud shadow. In this chapter, we reviewed many automated cloud and cloud shadow detection algorithms, which can provide guidance on the selection of algorithms for those interested in using LTS.

References

Ackerman, S. A., Strabala, K.I., Menzel, W. P., Frey, R. A., Moeller, C.C., and Gumley, L.E. 1998. Discriminating clear sky from clouds with MODIS. *Journal of Geophysical Research* 103(D24): 32141–32157. doi:10.1029/1998JD200032.

Berendes, T., Sengupta, S. K., Welch, R. M., Wielicki, B. A., and Navar, M. 1992. Cumulus cloud base height estimation from high spatial resolution Landsat data: A Hough transform approach. *IEEE Transactions on Geoscience and Remote Sensing* 30(3): 430–443. doi:10.1109/36.142921.

Braaten, J. D., Cohen, W. B., and Yang, Z. 2015. Automated cloud and cloud shadow identification in Landsat MSS imagery for temperate ecosystems. *Remote Sensing of Environment* 169: 128–138. doi:10.1016/j.rse.2015.08.006.

Chen, J. M. and Cihlar, J. 1996. Retrieving leaf area index of boreal conifer forests using Landsat TM images. *Remote Sensing of Environment* 55(2): 153–162. doi:10.1016/0034-4257(95)00195-6.

Chen, S., Chen, X., Chen, J., and Jia, P. 2015. An iterative haze optimized transformation for automatic cloud/haze detection of Landsat imagery. *IEEE Transactions on Geoscience and Remote Sensing* 54(5): 2682–2694. doi:10.1109/TGRS.2015.2504369.

Choi, H. and Bindschadler, R. 2004. Cloud detection in Landsat imagery of ice sheets using shadow matching technique and automatic normalized difference snow index threshold value decision. *Remote Sensing of Environment* 91(2): 237–242. doi:10.1016/j.rse.2004.03.007.

Collins, J. B. and Woodcock, C. E. 1996. An assessment of several linear change detection techniques for mapping forest mortality using multitemporal Landsat TM data. *Remote Sensing of Environment* 56(1): 66–77. doi:10.1016/0034-4257(95)00233-2.

Derrien, M., Farki, B., Harang, L., LeGleau, H., Noyalet, A., Pochic, D., and Sairouni, A. 1993. Automatic cloud detection applied to NOAA-11 /AVHRR imagery. *Remote Sensing of Environment* 46(3): 246–267. doi:10.1016/0034-4257(93)90046-Z.

Du, Y., Guindon, B., and Cihlar, J. 2002. Haze detection and removal in high resolution satellite image with wavelet analysis. *IEEE Transactions on Geoscience and Remote Sensing* 40(1): 210–217. doi:10.1109/36.981363.

Fan, C. N. and Zhang, F. Y. 2011. Homomorphic filtering based illumination normalization method for face recognition. *Pattern Recognition Letters* 32(10): 1468–1479. doi:10.1016/j.patrec.2011.03.023.

Fassnacht, K. S., Gower, S. T., MacKenzie, M. D., Nordheim, E. V., and Lillesand, T. M. 1997. Estimating the leaf area index of North Central Wisconsin forests using the Landsat thematic mapper. *Remote Sensing of Environment* 61(2): 229–245. doi:10.1016/S0034-4257(97)00005-9.

Foga, S., Scaramuzza, P. L., Guo, S., Zhu, Z., Dilley, R. D., Beckmann, T., Schmidt, G., Dwyer, J., Hughes, M., and Laue, B. 2017. Cloud detection algorithm comparison and validation for operational Landsat data products. *Remote Sensing of Environment* 194: 379–390. doi:10.1016/j.rse.2017.03.026.

Goodwin, N. R., Collett, L. J., Denham, R. J., Flood, N., and Tindall, D. 2013. Cloud and cloud shadow screening across Queensland, Australia: An automated method for Landsat TM/ETM+ time series. *Remote Sensing of Environment* 134: 50–65. doi:10.1016/j.rse.2013.02.019.

Gurney, C. M. 1982. The use of contextual information to detect cumulus clouds and cloud shadows in Landsat data. *International Journal of Remote Sensing* 3(1): 51–62. doi:10.1080/01431168208948379.

Hagolle, O., Huc, M., Pascual, D. V., and Dedieu, G. 2010. A multi-temporal method for cloud detection, applied to FORMOSAT-2, VENμS, LANDSAT and SENTINEL-2 images. *Remote Sensing of Environment* 114(8): 1747–1755. doi:10.1016/j.rse.2010.03.002.

Homer, C., Huang, C., Yang, L., Wylie, B., and Coan, M. 2004. Development of a 2001 national land-cover database for the United States. *Photogrammetric Engineering and Remote Sensing* 70(7): 829–840. doi:10.14358/PERS.70.7.829.

Huang, C. et al. 2010. Automated masking of cloud and cloud shadow for forest change analysis using Landsat images. *International Journal of Remote Sensing* 31(20): 5449–5464. doi:10.1080/01431160903369642.

Hughes, M. J. and Hayes, D. J. 2014. Automated detection of cloud and cloud shadow in single-date Landsat imagery using neural networks and spatial post-processing. *Remote Sensing of Environment* 6(6): 4907–4926. doi:10.3390/rs6064907.

Irish, R. R. 2000. Landsat 7 automatic cloud cover assessment. *Proceedings Volume 4049, Algorithms for Multispectral, Hyperspectral, and Ultraspectral Imagery*, Orlando, FL, United States, *AeroSense: International Society for Optics and Photonics*. doi:10.1117/12.410358.

Irish, R. R., Barker, J. L., Goward, S. N., and Arvidson, T. 2006. Characterization of the Landsat-7 ETM+ Automated Cloud-Cover Assessment (ACCA) algorithm. *Photogrammetric Engineering and Remote Sensing* 72(10): 1179–1188. doi:10.14358/PERS.72.10.1179.

Jin, S., Homer, C., Yang, L., Xian, G., Fry, J., Danielson, P., and Townsend, P. A. 2013. Automated cloud and shadow detection and filling using two-date Landsat imagery in the USA. *International Journal of Remote Sensing* 34(5): 1540–1560. doi:10.1080/01431161.2012.720045.

Lee, J., Weger, R. C., Sengupta, S. K., and Welch, R. M. 1990. A neural network approach to cloud classification. *IEEE Transactions on Geoscience and Remote Sensing* 28(5): 846–855. doi:10.1109/36.58972.

Le Hégarat-Mascle, S. and André, C. 2009. Use of Markov random fields for automatic cloud/shadow detection on high resolution optical images. *ISPRS Journal of Photogrammetry and Remote Sensing* 64(4): 351–366. doi:10.1016/j.isprsjprs.2008.12.007.

Li, Q., Lu, W., Yang, J., and Wang, J. Z. 2012. Thin cloud detection of all-sky images using Markov random fields. *IEEE Geoscience and Remote Sensing Letters* 9(3): 417–421. doi:10.1109/LGRS.2011.2170953.

Liang, S., Fang, H., and Chen, M. 2001. Atmospheric correction of Landsat ETM+ land surface imagery. I. Methods. *IEEE Transactions on Geoscience and Remote Sensing* 39(11): 2490–2498. doi:10.1109/36.964986.

Liu, C. B., Hu, J. B., Lin, Y., Wu, S. H., and Huang, W. 2011. Haze detection, perfection and removal for high spatial resolution satellite imagery. *International Journal of Remote Sensing* 32(23): 8685–8697. doi:10.1080/01431161.2010.547884.

Loveland, T. R. and Dwyer, J. L. 2012. Landsat: Building a strong future. *Remote Sensing of Environment* 122: 22–29. doi:10.1016/j.rse.2011.09.022.

Lu, D. 2005. Aboveground biomass estimation using Landsat TM data in the Brazilian Amazon. *International Journal of Remote Sensing* 26(12): 2509–2525. doi:10.1080/01431160500142145.

Luo, Y., Trishchenko, A. P., and Khlopenkov, K. V. 2008. Developing clear-sky, cloud and cloud shadow mask for producing clear-sky composites at 250-meter spatial resolution for the seven MODIS land bands over Canada and North America. *Remote Sensing of Environment* 112(12): 4167–4185. doi:10.1016/j.rse.2008.06.010.

Martins, J. V., Tanré, D., Remer, L., Kaufman, Y., Mattoo, S., and Levy, R. 2002. MODIS cloud screening for remote sensing of aerosols over oceans using spatial variability. *Geophysical Research Letters* 29(12): MOD4-1–MOD4-4. doi:10.1029/2001GL013252.

Oreopoulos, L., Wilson, M. J., and Várnai, T. 2011. Implementation on Landsat data of a simple cloud-mask algorithm developed for MODIS land bands. *IEEE Geoscience and Remote Sensing Letters* 8(4): 597–601. doi:10.1109/LGRS.2010.2095409.

Pflugmacher, D., Cohen, W. B., and Kennedy, R. E. 2012. Using Landsat-derived disturbance history (1972–2010) to predict current forest structure. *Remote Sensing of Environment* 122: 146–165. doi:10.1016/j.rse.2011.09.025.

Potapov, P., Turubanova, S., and Hansen, M. C. 2011. Regional-scale boreal forest cover and change mapping using Landsat data composites for European Russia. *Remote Sensing of Environment* 115(2): 548–561. doi:10.1016/j.rse.2010.10.001.

Qiu, S., He, B., Zhu, Z., Liao Z., and Quan, X. 2017. Improving Fmask cloud and cloud shadow detection in mountainous area for Landsats 4–8 images. *Remote Sensing of Environment* 199: 107–119. doi:10.1016/j.rse.2017.07.002.

Richter, R. 1996. A spatially adaptive fast atmospheric correction algorithm. *International Journal of Remote Sensing* 17(6): 1201–1214. doi:10.1080/01431169608949077.

Roy, D. P., Ju, J., Kline, K., Scaramuzza, P. L., Kovalskyy, V., Hansen, M., Loveland, T. R., Vermote, E., and Zhang, C. 2010. Web-enabled Landsat Data (WELD): Landsat ETM+ composited mosaics of the conterminous United States. *Remote Sensing of Environment* 114(1): 35–49. doi:10.1016/j.rse.2009.08.011.

Scaramuzza, P. L., Bouchard, M. A., and Dwyer, J. L. 2012. Development of the Landsat data continuity mission cloud-cover assessment algorithms. *IEEE Transactions on Geoscience and Remote Sensing* 50(4): 1140–1154. doi:10.1109/TGRS.2011.2164087.

Selkowitz, D. J. and Forster, R. R. 2015. An automated approach for mapping persistent ice and snow cover over high latitude regions. *Remote Sensing* 8(1): 16. doi:10.3390/rs8010016.

Shen, H., Li, H., Qian, Y., Zhang, L., and Yuan, Q. 2014. An effective thin cloud removal procedure for visible remote sensing images. *ISPRS Journal of Photogrammetry and Remote Sensing* 96: 224–235. doi:10.1016/j.isprsjprs.2014.06.011.

Simpson, J. J., Jin, Z., and Stitt, J. R. 2000. Cloud shadow detection under arbitrary viewing and illumination conditions. *IEEE Transactions on Geoscience and Remote Sensing* 38(2): 972–976. doi:10.1109/36.841979.

Sun, L. et al. 2016. A universal dynamic threshold cloud detection algorithm (UDTCDA) supported by a prior surface reflectance database. *Journal of Geophysical Research: Atmospheres* 121(12): 7172–7196. doi:10.1002/2015JD024722.

U.S. Geological Survey. 2016a. L7 Irish Cloud Validation Masks. *U.S. Geological Survey data release*. doi:10.5066/F7XD0ZWC. (accessed September 26, 2017)

U.S. Geological Survey. 2016b. L8 SPARCS Cloud Validation Masks. *U.S. Geological Survey data release*. doi:10.5066/F7FB5146. (accessed September 26, 2017)

U.S. Geological Survey. 2016c. L8 Biome Cloud Validation Masks. *U.S. Geological Survey data release*. doi:10.5066/F7251GDH. (accessed September 26, 2017)

Vermote, E., Justice, C., Claverie, M., and Franch, B. 2016. Preliminary analysis of the performance of the Landsat 8/OLI land surface reflectance product. *Remote Sensing of Environment* 185: 46–56. doi:10.1016/j.rse.2016.04.008.

Vermote, E. and Saleous, N. 2007. *LEDAPS Surface Reflectance Product Description*. College Park: University of Maryland. doi:null

Wang, B., Ono, A., Muramatsu, K., and Fujiwara, N. 1999. Automated detection and removal of clouds and their shadows from Landsat TM images. *IEICE Transactions on Information and Systems* 82(2): 453–460. doi:null

Wilson, M. J. and Oreopoulos, L. 2013. Enhancing a simple MODIS CLOUD mask algorithm for the Landsat data continuity mission. *IEEE Transactions on Geoscience and Remote Sensing* 51(2): 723–731. doi:10.1109/TGRS.2012.2203823.

Woodcock, C. E. et al. 2008. Free access to Landsat imagery, *Science* 320: 1011–1012. doi:10.1126/science.320.5879.1011a.

Wulder, M. A., Masek, J. G., Cohen, W. B., Loveland, T. R., and Woodcock, C. E. 2012. Opening the archive: How free data has enabled the science and monitoring promise of Landsat. *Remote Sensing of Environment* 122: 2–10. doi:10.1016/j.rse.2012.01.010.

Wulder, M. A., White, J. C., Loveland, T. R., Woodcock, C. E., Belward, A. S., Cohen, W. B., Fosnight, E. A., Shaw, J., Masek, J. G., and Roy, D. P. 2016. The global Landsat archive: Status, consolidation, and direction. *Remote Sensing of Environment* 185: 271–283. doi:10.1016/j.rse.2015.11.032.

Xian, G., Homer, C., and Fry, J. 2009. Updating the 2001 National Land Cover Database land cover classification to 2006 by using Landsat imagery change detection methods. *Remote Sensing of Environment* 113(6): 1133–1147. doi:10.1016/j.rse.2009.02.004.

Yuan, F., Sawaya, K. E., Loeffelholz, B. C., and Bauer, M. E. 2005. Land cover classification and change analysis of the Twin Cities (Minnesota) Metropolitan Area by multitemporal Landsat remote sensing. *Remote Sensing of Environment* 98(2): 317–328. doi:10.1016/j.rse.2005.08.006.

Zhang, Y., Guindon, B., and Cihlar, J. 2002. An image transform to characterize and compensate for spatial variations in thin cloud contamination of Landsat images. *Remote Sensing of Environment* 82(2): 173–187. doi:10.1016/S0034-4257(02)00034-2.

Zheng, D., Rademacher, J., Chen, J., Crow, T., Bresee, M., Le Moine, J., and Ryu, S. R. 2004. Estimating aboveground biomass using Landsat 7 ETM+ data across a managed landscape in northern Wisconsin, USA. *Remote Sensing of Environment* 93(3): 402–411. doi:10.1016/j.rse.2004.08.008.

Zhou, G., Zhou, X., Yue, T., and Liu, Y. 2016. An optional threshold with SVM cloud detection algorithm and DSP implementation. *ISPRS-International Archives of the Photogrammetry, Remote Sensing and Spatial Information Sciences* 41: 771–777. doi:10.5194/isprs-archives-XLI-B8-771-2016.

Zhu, Z. and Woodcock, C. E. 2012. Object-based cloud and cloud shadow detection in Landsat imagery. *Remote Sensing of Environment* 118: 83–94. doi:10.1016/j.rse.2011.10.028.

Zhu, Z. and Woodcock, C. E. 2014. Automated cloud, cloud shadow, and snow detection in multitemporal Landsat data: An algorithm designed specifically for monitoring land cover change. *Remote Sensing of Environment* 152: 217–234. doi:10.1016/j.rse.2014.06.012.

Zhu, Z., Wang, S., and Woodcock, C. E. 2015. Improvement and expansion of the Fmask algorithm: Cloud, cloud shadow, and snow detection for Landsats 4–7, 8, and Sentinel 2 images. *Remote Sensing of Environment* 159: 269–277. doi:10.1016/j.rse.2014.12.014.